Cancer Nanotechnology

RESEARCH Open Access

In vivo imaging of prostate tumor-targeted folic acid conjugated quantum dots

Sulaxna Pandey[1,2], Prakash Choudhary[1], Virendra Gajbhiye[1,2], Sachin Jadhav[1,2] and Dhananjay Bodas[1,2*]

*Correspondence:
Dhananjay Bodas
dsbodas@aripune.org
[1]Nanobioscience Group, Agharkar Research Institute, GG Agarkar Road, 411 004 Pune, India
[2]Savitribai Phule Pune University, Ganeshkhind Road, 411 007 Pune, India

Abstract

Cancer is a major threat to human health; thus, early detection is imperative for successful management. Rapid diagnosis can be achieved by imaging primary (subcutaneous) tumors using fluorophores conjugated with tumor markers. Here, the application of biocompatible, quantum efficient, monodisperse, and photostable polymer-coated quantum dots (PQDs) is demonstrated for targeted prostate tumor imaging in living SCID mice. Briefly, PQDs (blue) are conjugated to folic acid (FA-PQDs) using DCC-NHS chemistry. Initially, in vitro targeted imaging via FA-PQDs is evaluated in LNCaP cells. The confocal microscopic evaluation demonstrates the uptake of FA-PQDs. To understand the dispersion of PQDs in vivo, the biodistribution of PQDs is assessed at different time intervals (1- 180 min) using whole-body fluorescence imaging and computed tomography (CT) scan. PQDs are seen to accumulate in organs like the liver, kidneys, spleen, lungs, and urinary bladder within 60 min, however, PQDs are not observed at 180 min indicating renal clearance. Further, to target the prostate tumor (~200 mm^3) in mice, FA-PQDs are injected intravenously, and whole-body fluorescence imaging along with a CT scan is recorded. FA-PQDs are seen at the tumor site as compared to PQDs. The results confirm that the FA-PQDs function as excellent nanoprobes for targeted tumor imaging in vivo.

Keywords *In vivo*, Whole-body fluorescence imaging, Tumor imaging, Prostate tumor, Quantum dots, CT scan

Introduction

Cancer is the leading cause of death worldwide, and it can be successfully treated when diagnosed in time. (Devi et al. 2022; Hoffman 2008; Pan and Feng 2009) Tumor imaging is well established and can be effective in early diagnosis. (Fass 2008; Liang et al. 2021; Lu et al. 2020; Younis et al. 2022) The existing techniques for tumor imaging consist of computed tomography (CT), magnetic resonance imaging (MRI), positron emission tomography (PET), etc. These techniques employ fluorophores for imaging tumors, however, the existing fluorophores suffer limitations in terms of photostability, quantum yield, and aqueous solubility. (McHugh et al. 2018; Mukhtar et al. 2020; Resch-Genger et al. 2008) Most commonly used Food and Drug Administration (FDA)-approved dyes

for cancer imaging are 5-aminolevulinic acid (5-ALA), methylene blue, and indocyanine green (for intraoperative tumor identification). (Azari et al. 2022; Chen et al. 2020; Weissleder and Pittet 2008; Wu et al. 2023; Zhang et al. 2017) 5-ALA is approved for fluorescence- guided surgery, but their excitation and emission wavelengths (405/645 nm) are heavily absorbed by tissue, thus, hindering the imaging depth. (Van Keulen et al. 2022; Weissleder and Pittet 2008; Zhang et al. 2017) Methylene blue is approved for sentinel lymph nodes (SLNs) mapping, but it possess potential toxicity for metabolic encephalopathy and exihibits a small stokes shift with largely overlapping spectra (668/688 nm). Thus, making it difficult to differentiate between excitation and emitted light. (Liu and Grodzinski 2021; Minamiya et al. 2009) Indocyanine green has comparatively favourable excitation and emission wavelength (807/822 nm), however, it suffers from poor thermal and photostability. (Chen et al. 2020; Minamiya et al. 2009; Resch-Genger et al. 2008; Zhang et al. 2017) Considering the limitations of existing dyes in imaging cancer, development of newer fluorescent probes with better fluorescence signal intensity, life time and photostability is essential. (Luo et al. 2022; Wagner et al. 2019)

Quantum dots are a unique class of fluorescent nanocrystals, that exhibit size tunable emission. They offer several advantages such as high photostability, quantum yield and aqueous solubility over traditional dyes. (Pandey et al. 2021; Pandey and Bodas 2020; Resch-Genger et al. 2008) Several researchers have reported the use of cancer biomarker labeled biocompatible QDs for targeted tumor imaging. Sun et al. (Sun et al. 2021) imaged H460 tumor-bearing mice using biocompatible Ag−In −S/ZnS quantum dots. Yang et al. (Yang et al. 2019) have reported tumor imaging in mice using Ag_2S quantum dots and graphene QDs respectively. Gao et al. (Gao et al. 2004a) described imaging of prostate tumor in mice using QD-PSMA.

The present study aims to demonstrate the suitability of biocompatible PQDs for targeted tumor imaging in living Severe combined immunodeficiency syndrome (SCID) mice. A detailed account of synthesis, characterization, and bioimaging application (in vitro and tissue) of PQDs is previously published. (Pandey et al. 2021) Here, PQDs are conjugated to folic acid (FA) to target folate receptors on cancer cells. The FA-PQDs is further used for in vitro targeted imaging of prostate cancer cells (LNCaP) and assessed by confocal microscopy. Furthermore, the biodistribution of PQDs is evaluated in vivo at different time intervals using a whole-body fluorescence imaging system and CT scan. Finally, FA-PQDs are targeted to demonstrate tumor imaging in SCID mice. For this, the prostate tumor is induced in the flank region of SCID mice by injecting LNCaP cells (10^7 cells/100 µL+100 µL Matrigel) subcutaneously. Finally, FA-PQDs are injected intravenously via tail vein in tumor-bearing SCID mice and the targeted tumor imaging is demonstrated using a whole-body imaging system and CT scan.

Experimental section

A detailed description of the microreactor-assisted synthesis process of PQDs along with its characterization is summarized in our published work. [12] Here, PQDs are characterized by photoluminescence (PL) spectroscopy (Hitachi F-2500) for emission wavelength. The emission wavelength of PQDs (1 mg/mL) is recorded at an excitation wavelength of 350 nm using photoluminescence (PL) spectroscopy. Further, MFP-3D Asylum Research Atomic Force Microscope (AFM) was used for the determination of size and its distribution. (Ali et al. 2018; Pandey et al. 2021)

Folic acid conjugation

Folic acid (FA-97%, 5 mg-11 μM) is dissolved in dimethyl sulfoxide (DMSO) followed by addition of N, N′-dicyclohexyl carbodiimide (DCC-99%, 2.5 mg-11 μM), and N-hydroxy succinimide (NHS- >95%, 1.2 mg-11 μM) in equal ratio. The reaction mixture is stirred under N_2 purging for 2 h at room temperature. Finally, the PQDs are added to the reaction mixture and allowed to react with carboxyl group activated folic acid under N_2 purging for 24 h. The folic acid conjugated PQDs (FA-PQDs) are purified by using a dialyzing membrane (1 kDa). (Gao et al. 2004b; Nair K et al. 2013) FTIR (IR Affinity-1, SHIMADZU) is used to confirm the conjugation.

In vitro cellular uptake of FA-PQDs

The prostate cancer (LNCaP) cells are procured from the National Center for Cell Science (NCCS, Pune, India) cell repository. LNCaP cell line is cultured in Roswell Park Memorial Institute Medium (RPMI 1640 media) supplemented with 10% fetal bovine serum (FBS) (Invitrogen, USA) and penicillin/streptomycin (Himedia). LNCaP cells are grown (10^4 cells/ well) on 6 well plates. Then, 100 μg of PQDs and, FA-PQDs are added separately followed by incubation in a CO_2 incubator for 1 h. Further, the cells are fixed and permeabilized via 4% paraformaldehyde (PFA) and 0.1% Triton X-100, respectively, followed by washing (1X PBS). Furthermore, rhodamine-phalloidin is added to stain the cytoskeleton and incubated for 40 min followed by washing (1X PBS). Finally, the stained cells are mounted on a glass slide and the imaging is carried out using confocal microscope (Leica SP8 with LasX software).

Biodistribution of PQDs

Institutional Animal Ethics committee (IAEC) (ARI/IEAC/2020/14) have approved the animal (32 SCID mice) work. The SCID mice are monitored regularly for food and growth based on the IAEC guidelines. After assessing the suitability of FA-PQDs in vitro, the biodistribution of PQDs in mice is evaluated. For this, Control and Test groups are created containing three mice (body weight: 20–25 g) each. Control and test groups are intravenously injected via tail vein with 1X PBS and PQDs (100 μg/ 100 μL-based on mice's 10 mg/kg body weight), respectively. Post injection, the mice are imaged using IVIS spectrum Perkin Elmer whole-body imaging system at different time intervals (1 min, 10 min, 30 min, 60 min, and 180 min). Further, the distribution of PQDs in various organs of mice is confirmed by CT scan (IVIS spectrum Perkin Elmer) at 180 min. The results obtained from whole-body imaging and CT scan are analyzed using IVIS imaging software.

In vivo prostate cancer imaging using FA-PQDs

SCID mice used for the study are regularly monitored for food and growth based on IAEC guidelines in the in-house animal facility. The prostrate tumor is induced in SCID mice by injecting LNCaP cells (10^7 cells/100 μL mixed with 100 μL of Matrigel) subcutaneously in the flank region. On tumor growth of ~200 mm^3, the mice are divided into 3 groups viz. control, non-targeted, and targeted, each comprising of 3 animals. For tumor imaging, mice of all the groups are injected intravenously via tail vein with 1X PBS, PQDs, and FA-PQDs, respectively, at a concentration of 1 mg/mL (100 μL). The whole-body fluorescence imaging of three groups is carried out at different time intervals (same

used in PQDs biodistribution study). The CT scan is recorded after 60 min (based on biodistribution study).

Results and discussion

PQDs characterization

The synthesized PQDs are characterized for their size by photoluminescence spectroscopy (PL) and atomic force microscopy (AFM). In Fig. 1a, the photoluminescence spectrum show the emission wavelength at 424 nm, suggesting the synthesis of blue PQDs (photograph shown in inset). Moreover, the 3D topographic image obtained using AFM shows the PQDs size distribution in the range of 1-3.5 nm (Fig. 1b).

Folic acid conjugation

PQDs are modified with folic acid to target folate receptors on cancer cells. Folic acid, due to its properties of non-immunogenicity, high stability, tissue permeability, low molecular weight, and easy conjugation to diverse types of nanoparticles, makes them an ideal choice to target folate receptor on cancer cells. Thus, folic acid is conjugated to PQDs using DCC-NHS chemistry. (Gao et al. 2004b; Jeena et al. 2019) The scheme for the conjugation process is shown in Fig. 2a. FTIR spectra seen in Fig. 2b confirms the conjugation of folic acid to PQDs wherein peaks at 795 cm^{-1}, 890 cm^{-1}, 925 cm^{-1}, 1000 cm^{-1}, 1377 cm^{-1}, 2293 cm^{-1}, 2970 cm^{-1}, and 3544 cm^{-1} corresponds to Si-CH_3, C-NH_2, C–O vibration, symmetric carboxylic vibrations, Si–O–Si, C=C, O–CH_3 stretching vibration, and free OH, respectively. The amide bond located at peak position of 1640 cm^{-1} and 1430 cm^{-1} corresponding to -CO-NH_2 and -CONH, respectively (Fig. 2b), confirm the folic acid conjugation to PQDs. (Gao et al. 2004b; Nair K et al. 2013; Suriamoorthy et al. 2010)

In vitro cellular uptake

LNCaP cells treated with PQDs and FA-PQDs are assessed for their cellular uptake of non-targeted and targeted groups, respectively using confocal microscopy. In Fig. 3, the upper panel shows the LNCaP cells treated with rhodamine-phalloidin (red) and PQDs. It can be seen that very few PQDs are internalized in the cell membrane. In contrast, FA-PQDs (shown in lower panel) are internalized in higher amounts owing to folate receptor-mediated pathway. The merged image of the targeted imaging panel showed magenta color due to colocalization of FA-PQDs (blue) and rhodamine-phalloidin (red).

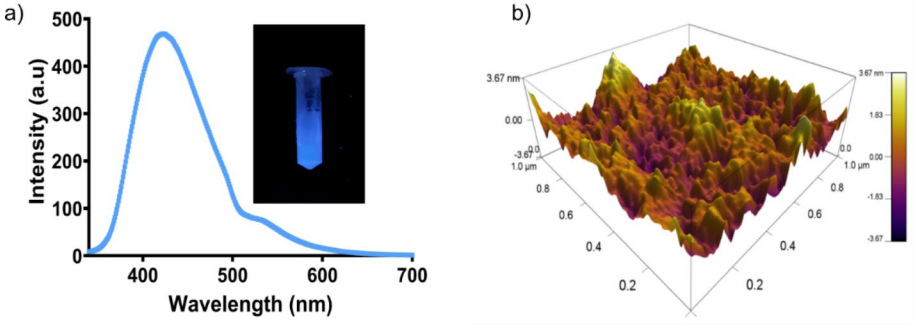

Fig. 1 (a) Photoluminescence spectrum showing the emission wavelength of PQDs; inset shows the synthesized blue PQDs (b) AFM topographic 3D image of blue color PQDs.

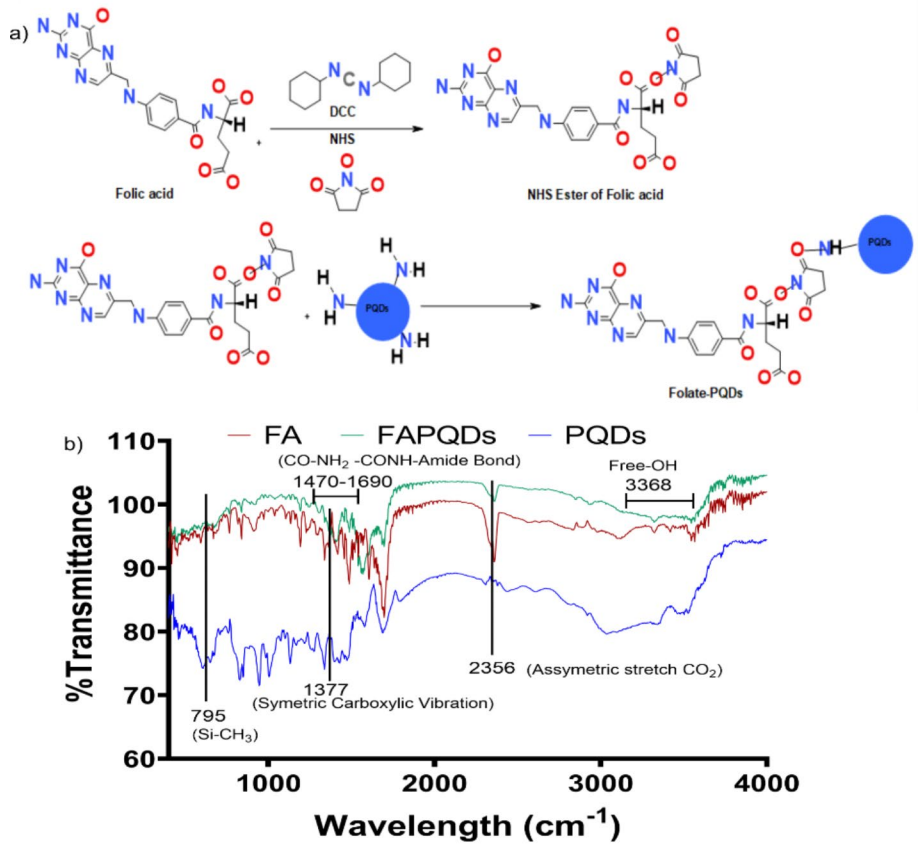

Fig. 2 (a) Scheme shows the schematic of FA conjugation with PQDs using DCC-NHS chemistry. (b) FTIR spectra of free FA, PQDs and FA conjugated PQDs

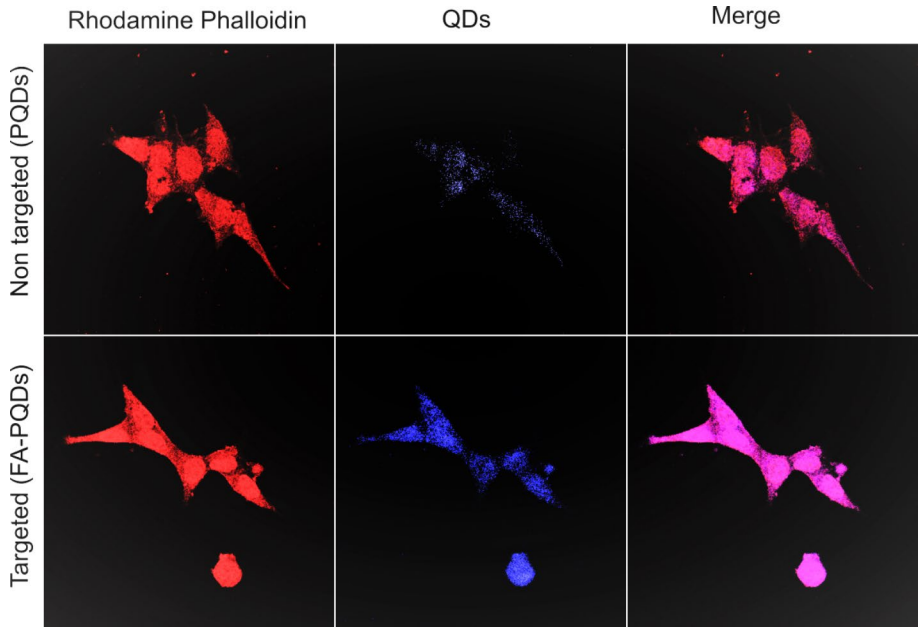

Fig. 3 Confocal microscopy images for cellular uptake of PQDs and FA-conjugated PQDs in LNCaP cells

However, in the non-targeted panel, the merged image appears red as fewer PQDs are present. Moreover, the ImageJ software measurement of FA-PQDs (95,424) uptake in LNCaP cells shows the higher particle number compared to PQDs (35,948). Thus, suitability of FA-PQDs to target cancer cells in vitro is demonstrated.

In vivo PQDs biodistribution

The biodistribution of PQDs is assessed by whole-body fluorescence imaging and CT scan. The whole-body fluorescence imaging of control (1X PBS) and test (PQDs) is recorded at different time intervals. In Fig. 4a, the whole-body fluorescence imaging of test and control at different time intervals shows high fluorescence of test mice compared to control group (See supplementary movies 1–2). The fluorescence intensity recorded with time for PQDs is plotted, and the significance of the distribution of PQDs at different time intervals is assessed. As seen in Fig. 4b, the fluorescence intensity of PQDs at 1 min was significantly higher ($P^{**} < 0.05$) than the intensity obtained after 180 min suggesting renal clearance. To further see the distribution of PQDs in organs, a CT scan at 180 min is recorded. The CT scan of control mice shows autofluorescence in different organs. The CT scan of test mice shows low intensity (blue on scale bar) fluorescence indicating sparse distribution of PQDs in organs such as the kidney, lungs, spleen and liver (Fig. 4c). However, PQDs are seen to accumulate near the urinary bladder with a high intensity (red on scale bar) fluorescence confirming renal clearance at 180 min.

In vivo tumor imaging

After assessing the cellular uptake of FA-PQDs in LNCaP cells, their use was finally evaluated in targeted imaging of prostate tumors in mice. 3 groups viz. Control, Non-targeted, and Targeted are intravenously injected with 1X PBS, PQDs, and FA-PQDs respectively, via tail vein of the mice and observed by whole-body fluorescence imaging

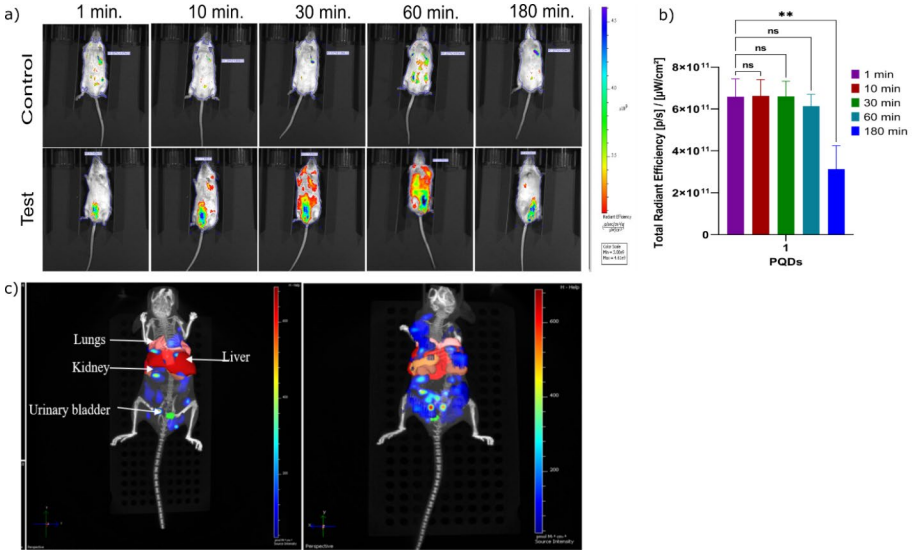

Fig. 4 (a) Whole-body fluorescence imaging of control and test group at different time intervals. (b) Graph shows the significance of fluorescence intensity of PQDs distribution with respect to control group at different time intervals (2-Way ANOVA-multiple comparison Dunnet test). (c) CT scan image of control and test group showing the distribution of PQDs in different organs of mice

and CT scan. Targeted group show higher fluorescence intensity at the tumor site as compared to the other groups (Fig. 5a and please see supplementary movie 3–5) indicated targeted delivery of FA-PQDs. Moreover, a time-dependent increase in fluorescence intensity is observed near the tumor site. Dunnet's test shows no significance between the non-targeted and targeted groups upto 30 min (Fig. 5b). However, after 60 min, fluorescence intensity of targeted group is seen to be significantly higher (**$P < 0.05$) than non-targeted group. At 180 min time point, the targeted group shows significantly higher fluorescence intensity as compared to non-targeted group, suggesting accumulation of FA-PQDs at the tumor site. Thus, the higher fluorescence intensity observed in tumor of targeted group suggests the specific uptake of FA-PQDs corresponding to folate receptor mediated pathway. (Deng et al. 2012)

To confirm the accumulation of FA-PQDs specifically within the tumor, a CT scan of the tumor is recorded at 60 min time point. The CT scan (Fig. 5c) clearly shows maximum accumulation of FA-PQDs (blue on scale bar) within the tumor. In contrast, the control and non-targeted group showed low or no fluorescence at the tumor site. Thus, it is evident from the whole-body fluorescence imaging and CT scan that FA-PQDs can be potentially used for cancer imaging in vivo.

Discussion

Biocompatible, quantum efficient and photostable QDs are an ideal choice for in vitro and in vivo imaging applications. These properties are essential for bioimaging applications especially for in vivo imaging.

In the present study, biocompatible, quantum efficient and photostable PQDs (reported previously) (Pandey et al. 2021) are modified with folic acid to target prostate tumor in tumor bearing SCID mice. The evaluation of tumor targeted imaging in live

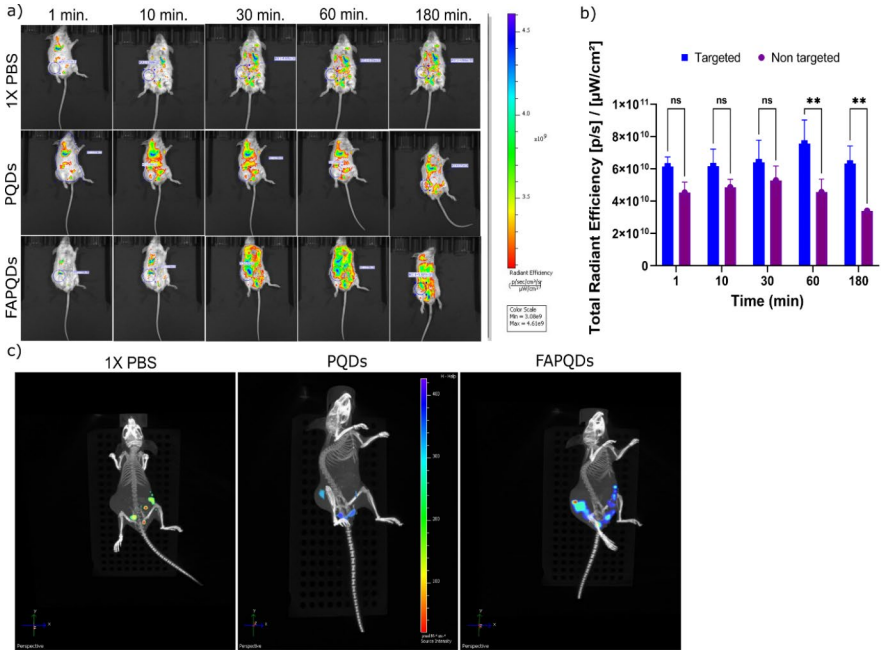

Fig. 5 (a) whole-body fluorescence tumor imaging of control, non-targeted and targeted groups of SCID mice at different time intervals. (b) Graph showing the significance of tumor fluorescence intensity of targeted group with control and non-targeted groups (2-Way ANOVA-multiple comparison Dunnet's test). (c) CT scan image of control, non-targeted and targeted groups at 60 min

SCID mice was done by whole-body fluorescence imaging and computed tomography scan.

The PQDs (blue color) were synthesized using the reported method (Pandey et al. 2021). They were characterized for their size by photoluminescence spectroscopy (PL) and atomic force microscopy (AFM). In Fig. 1a, the photoluminescence spectrum and AFM showed the emission wavelength at 424 nm, suggesting the synthesis of blue PQDs (photograph shown in inset) and size distribution in the range of 1-3.5 nm (Fig. 1b) respectively. (Ali et al. 2018; Pandey et al. 2021) PQDs were further modified with folic acid using DCC-NHS coupling chemistry (Scheme of Fig. 2a). (Gao et al. 2004b; Nair K et al. 2013) The FTIR spectra showed peaks at 1640 cm^{-1} and 1430 cm^{-1} corresponding to -CO-NH_2 and -CONH, respectively (Fig. 2b) confirming the folic acid conjugation of PQDs.(Liu et al. 2018; Suriamoorthy et al. 2010).

Further, the folic acid modified PQDs (FA-PQDs) were used for in vitro targeted imaging of LNCaP cells (prostate cancer). The in vitro cancer targeted imaging of LNCaP cells using FA-PQDs was demonstrated via confocal microscopy. The confocal microscopy images revealed the higher localization of FA-PQDs within the cell membrane of LNCaP cells owing to folate receptor-mediated pathway. (Bharali et al. 2005; Gao et al. 2004b; Kadian et al. 2020; Wang et al. 2014) In contrast, very less accumulation of the non-targeted group (PQDs) was seen (Fig. 3). Also, the ImageJ software measurement of FA-PQDs (95,424) uptake in LNCaP cells shows the higher particle number compared to PQDs (35,948). Therefore, confirming the targetability of FA-PQDs.

Furthermore, the biodistribution of PQDs within the living SCID mice was assessed at different time intervals using whole-body fluorescence imaging system (Fig. 4a). The fluorescence intensity recorded with time for PQDs is plotted, and the significance of the distribution of PQDs at different time intervals was assessed. As seen in Fig. 4b, the fluorescence intensity of PQDs at 1 min was significantly higher ($P^{**} < 0.05$) than the intensity obtained after 180 min suggesting renal clearance. To further see the distribution of PQDs in organs, a CT scan at 180 min is recorded. The study showed the distribution of PQDs in the organs like kidney, lungs, spleen and liver and higher accumulation was seen within the urinary bladder (Fig. 4c andsupplementary movies 1& 2), which further indicate the renal clearance at 180 min.

Finally, FA-PQDs were used to target prostrate tumor in tumor bearing living SCID mice. Tumor was induced in SCID mice by injecting LNCaP cells subcutaneously in the flank region. Tumor volume when reaches upto 200 mm^3, mice were divided into three groups (Targeted, Non-targeted and Control). The targeted, non-targeted and control groups were injected with FA-PQDs, PQDs and 1X PBS respectively. The whole-body fluorescence imaging showed higher fluorescence intensity at the tumor site within the targeted group as compared to the other groups (Fig. 5a and supplementary movies 3–5). Moreover, time dependent accumulation of FA-PQDs revealed an increase in fluorescence intensity at the tumor site. Further, Dunnet's test shows no significance between the non-targeted and targeted groups upto 30 min (Fig. 5b). This may be due to the insufficient time for the FA-PQDs to target the tumor cells. However, after 60 min, fluorescence intensity of targeted group is seen to be significantly higher ($^{**}P < 0.05$) than non-targeted group. This can be attributed to the accumulation of FA-PQDs via receptor targeted pathway within the tumor. The result is in good agreement to the biodistribution data (Fig. 4b). Furthermore, possibility of renal clearance of PQDs (refer

to biodistribution data) at 180 min might be a contributing factor for the higher significance of targeted group. To further confirm the accumulation of FA-PQDs within the tumor, CT scan at 60 min was recorded. The CT scan (Fig. 5c) evidently shows higher accumulation of FA-PQDs within the tumor. In contrast, the control and non-targeted group showed low or no fluorescence at the tumor site. Thus, the whole-body fluorescence imaging and CT scan evidently showed the potentiality of FA-PQDs for cancer imaging in vivo.

Conclusion

PQDs are successfully modified with folic acid (FA-PQDs) for folate receptor-mediated target imaging of prostate cancer cells. The confocal microscopy reveals effectual cellular uptake of FA-PQDs in LNCaP cells. Thus, confirming the suitability of FA-PQDs in targeting cancer cells via a receptor-mediated pathway. Furthermore, biodistribution of PQDs in mice using whole-body fluorescence imaging and CT scan reveals the maximum accumulation of PQDs in organs like kidney, liver, lungs, spleen and urinary bladder within 60 min. Moreover, most of the PQDs are observed within the urinary bladder at 180 min suggesting renal clearance. Furthermore, the FA-PQDs are used for cancer-targeted imaging in mice. Whole-body fluorescence imaging and CT scan indicates the accumulation of FA-PQDs at the tumor site. Therefore, the suitability of PQDs in tumor imaging of living mice is demonstrated successfully. The present study establishes the use of PQDs for targeting subcutaneous imaging of prostate tumors in living mice. Thus, making QDs a good alternative for cancer diagnosis to existing fluorescent dyes. These PQDs can be conjugated with different cancer-specific biomarkers for cancer imaging in vivo. Moreover, the PQDs can be conjugated to cancer-specific drugs for the targeted treatment of cancer.

Supplementary Information

The online version contains supplementary material available at https://doi.org/10.1186/s12645-023-00162-1.

Supplementary Material 1

Supplementary Material 2

Supplementary Material 3

Supplementary Material 4

Supplementary Material 5

Acknowledgements

Sulaxna Pandey gratefully acknowledges the fellowship from the Indian Council of Medical Research-SRF (ISRM/11(73)/2017). Authors thank the help and support extended by Dr. Santra and Dr. Bopanna, Animal house, National Center for Cell Science, Pune for whole body imaging.

Author Contribution

SP conducted all the experiments. SP analyzed the data and wrote the mauuscript. PC helped in LNCaP cell growth and maintenance. VG helped in the analysis of data and manuscript writing. SJ helped during animal experiments. DB designed and conceptualized the study. DB helped in the analysis of all the data obtained from the experiments, writing and finalizing the manuscript.

Funding

No funding was available for the work.

Data Availability

All data generated or analysed during this study are included in this published article (and its supplementary information files).

Declarations

Conflict of Interest

The authors declare that they have no known competing financial interests or personal relationships that could have appeared to influence the work reported in this paper.

Consent for publication

All authors have read and approved the manuscript for submission and publication.

Ethical approval

The Institutional animal ethical committee (IAEC) approval (Approval number: ARI/IAEC/2020/14 dated: 07 October 2020) was taken from our institure before the initiation of the work.

Received: 11 October 2022 / Accepted: 4 February 2023

Published online: 30 March 2023

References

Ali M, El Nady J, Ebrahim S, Soliman M (2018) Structural and optical properties of upconversion CuInS/ZnS quantum dots. Opt. Mater. (Amst). [Internet]. Elsevier; ;86(September):545–9. Available from: https://doi.org/10.1016/j.optmat.2018.10.058

Azari F, Zhang K, Kennedy GT, Chang A, Nadeem B, Delikatny EJ et al (2022) Precision Surgery Guided by Intraoperative Molecular Imaging. J. Nucl. Med. [Internet]. Nov 11;63(11):1620–7. Available from: http://jnm.snmjournals.org/lookup/doi/https://doi.org/10.2967/jnumed.121.263409

Bharali DJ, Lucey DW, Jayakumar H, Pudavar HE, Prasad PN (2005) Aug;127(32):11364–71 Folate-Receptor-Mediated Delivery of InP Quantum Dots for Bioimaging Using Confocal and Two-Photon Microscopy. J. Am. Chem. Soc. [Internet]. Available from: https://doi.org/10.1021/ja051455x

Chen M, Feng S, Yang Y, Li Y, Zhang J, Chen S et al (2020) Tracking the in vivo spatio-temporal patterns of neovascularization via NIR-II fluorescence imaging. Nano Res. [Internet]. Nov 10;13(11):3123–9. Available from: https://link.springer.com/https://doi.org/10.1007/s12274-020-2982-7

Deng D, Chen Y, Cao J, Tian J, Qian Z, Achilefu S et al (2012) High-Quality CuInS 2 /ZnS Quantum Dots for In vitro and In vivo Bioimaging. Chem. Mater. [Internet]. Aug 14;24(15):3029–37. Available from: https://doi.org/10.1021/cm3015594

Devi S, Kumar M, Tiwari A, Tiwari V, Kaushik D, Verma R et al (2022) Quantum Dots: An Emerging Approach for Cancer Therapy. Front. Mater. [Internet]. Jan 10;8(January):1–18. Available from: https://www.frontiersin.org/articles/https://doi.org/10.3389/fmats.2021.798440/full

Fass L (2008) Aug;2(2):115–52 Imaging and cancer: A review. Mol. Oncol. [Internet]. Available from: http://doi.wiley.com/https://doi.org/10.1016/j.molonc.2008.04.001

Gao X, Cui Y, Levenson RM, Chung LWK, Nie S (2004a) In vivo cancer targeting and imaging with semiconductor quantum dots. Nat Biotechnol 22(8):969–976

Gao X, Cui Y, Levenson RM, Chung LWK, Nie S (2004b) In vivo cancer targeting and imaging with semiconductor quantum dots. Nat. Biotechnol. [Internet]. Royal Society of Chemistry; Aug 18;22(8):969–76. Available from: http://xlink.rsc.org/?DOI=C9RA01435G

Hoffman AS (2008) The early history of Nanocarriers as Drug Delivery Systems Nanomedicine for molecular imaging: interest of bimodality in preclinical studies. p.135–53

Jeena K, Manju CA, Sajesh KM, Gowd GS, Sivanarayanan TB, Mol CD et al (2019) Brain-Tumor-Regenerating 3D Scaffold-Based Primary Xenograft Models for Glioma Stem Cell Targeted Drug Screening. ACS Biomater. Sci. Eng. [Internet]. American Chemical Society; Jan 14;5(1):139–48. Available from: https://doi.org/10.1021/acsbiomaterials.8b00249

Kadian S, Manik G, Das N, Roy P (2020) Targeted bioimaging and sensing of folate receptor-positive cancer cells using folic acid-conjugated sulfur-doped graphene quantum dots. Microchim. Acta [Internet]. Microchimica Acta; Aug 18;187(8):458. Available from: https://link.springer.com/https://doi.org/10.1007/s00604-020-04448-8

Van Keulen S, Hom M, White H, Rosenthal EL, Baik FM (2022) The Evolution of Fluorescence-Guided Surgery. Mol. Imaging Biol. [Internet]. Springer International Publishing; ;(0123456789). Available from: https://doi.org/10.1007/s11307-022-01772-8

Liang Z, Khawar MB, Liang J, Sun H (2021) Bio-Conjugated Quantum Dots for Cancer Research: Detection and Imaging. Front. Oncol. [Internet]. Oct 22;11(October):1–14. Available from: https://www.frontiersin.org/articles/https://doi.org/10.3389/fonc.2021.749970/full

Liu CH, Grodzinski P (2021) Nanotechnology for Cancer Imaging: Advances, Challenges, and Clinical Opportunities. Radiol. Imaging cancer [Internet]. May 1;3(3):e200052. Available from: https://doi.org/10.1148/rycan.2021200052

Liu H, Li Z, Sun Y, Geng X, Hu Y, Meng H, Springer US et al (2018) ; Dec 18;8(1):1086. Available from: https://doi.org/10.1038/s41598-018-19373-3

Lu F, Ju W, Zhao N, Zhao T, Zhan C, Wang Q et al (2020) Sep;529(4):930–5 Aqueous synthesis of PEGylated Ag2S quantum dots and their in vivo tumor targeting behavior. Biochem. Biophys. Res. Commun. [Internet]. Elsevier Ltd; Available from: https://doi.org/10.1016/j.bbrc.2020.06.072

Luo M, Yukawa H, Baba Y (2022) Micro-/nano-fluidic devices and in vivo fluorescence imaging based on quantum dots for cytologic diagnosis. Lab Chip [Internet]. Royal Society of Chemistry; ;22(12):2223–36. Available from: http://xlink.rsc.org/?DOI=D2LC00113F

McHugh KJ, Jing L, Behrens AM, Jayawardena S, Tang W, Gao M et al (2018) May;30(18):1706356 Biocompatible Semiconductor Quantum Dots as Cancer Imaging Agents. Adv. Mater. [Internet]. Available from: https://onlinelibrary.wiley.com/doi/https://doi.org/10.1002/adma.201706356

Minamiya Y, Saito H, Ito M, Motoyama S, Katayose Y, Ogawa J Radio-guided thoracoscopic surgery with 99mTc-methoxy-isobutylisonitrile for treating an ectopic mediastinal parathyroid adenoma in an adolescent girl. Gen. Thorac. Cardiovasc. Surg. [Internet]. 2009 Dec 15;57(12):657–9. Available from: http://link.springer.com/https://doi.org/10.1007/s11748-009-0458-5

Mukhtar M, Bilal M, Rahdar A, Barani M, Arshad R, Behl T et al (2020) Nanomaterials for Diagnosis and Treatment of Brain Cancer: Recent Updates. Chemosensors [Internet]. Nov 20;8(4):117. Available from: https://www.mdpi.com/2227-9040/8/4/117

Nair KL, Jagadeeshan S, Nair SA, Kumar GSV (2013) Folic Acid Conjugated δ-Valerolactone-Poly(ethylene glycol) Based Triblock Copolymer as a Promising Carrier for Targeted Doxorubicin Delivery. Lorenz C, editor. PLoS One [Internet]. Aug 21;8(8):e70697. Available from: https://doi.org/10.1371/journal.pone.0070697

Pan J, Feng S-S (2009) Feb;30(6):1176–83 Targeting and imaging cancer cells by Folate-decorated, quantum dots (QDs)- loaded nanoparticles of biodegradable polymers. Biomaterials [Internet]. Elsevier Ltd; Available from: https://doi.org/10.1016/j.biomaterials.2008.10.039

Pandey S, Bodas D (2020) Apr;278:102137 High-quality quantum dots for multiplexed bioimaging: A critical review. Adv. Colloid Interface Sci. [Internet]. Elsevier B.V.; Available from: https://doi.org/10.1016/j.cis.2020.102137

Pandey S, Mukherjee D, Kshirsagar P, Patra C, Bodas D (2021) Multiplexed bio-imaging using cadmium telluride quantum dots synthesized by mathematically derived process parameters in a continuous flow active microreactor. Mater. Today Bio [Internet]. Elsevier Ltd; ;11(June):100123. Available from: https://doi.org/10.1016/j.mtbio.2021.100123

Resch-Genger U, Grabolle M, Cavaliere-Jaricot S, Nitschke R, Nann T (2008) Quantum dots versus organic dyes as fluorescent labels.Nat. Methods. p.763–75

Sun X, Shi M, Zhang C, Yuan J, Yin M, Du S et al (2021) Fluorescent Ag–In–S/ZnS Quantum Dots for Tumor Drainage Lymph Node Imaging In Vivo. ACS Appl. Nano Mater. [Internet]. Feb 26;4(2):1029–37. Available from: https://doi.org/10.1021/acsanm.0c02542

Suriamoorthy P, Zhang X, Hao G, Joly AG, Singh S, Hossu M et al (2010) Folic acid-CdTe quantum dot conjugates and their applications for cancer cell targeting. Cancer Nanotechnol. [Internet]. Dec 31;1(1–6):19–28. Available from: https://cancer-nano.biomedcentral.com/articles/https://doi.org/10.1007/s12645-010-0003-3

Wagner AM, Knipe JM, Orive G, Peppas NA (2019) Quantum dots in biomedical applications. Acta Biomater. [Internet]. Acta Materialia Inc.; ;94:44–63. Available from: https://doi.org/10.1016/j.actbio.2019.05.022

Wang X, Sun X, Lao J, He H, Cheng T, Wang M et al (2014) Multifunctional graphene quantum dots for simultaneous targeted cellular imaging and drug delivery. Colloids Surfaces B Biointerfaces [Internet]. Elsevier B.V.; ;122:638–44. Available from: https://doi.org/10.1016/j.colsurfb.2014.07.043

Weissleder R, Pittet MJ Imaging in the era of molecular oncology. Nature [Internet]. 2008 Apr 2;452(7187):580–9. Available from: http://www.nature.com/articles/nature06917

Wu R, Wang K, Gai Y, Li M, Wang J, Wang C et al (2023) Nanomedicine for renal cell carcinoma: imaging, treatment and beyond. J. Nanobiotechnology [Internet]. BioMed Central; ;21(1):3. Available from: https://doi.org/10.1186/s12951-022-01761-7

Yang Y, Chen S, Li H, Yuan Y, Zhang Z, Xie J et al (2019) Engineered Paramagnetic Graphene Quantum Dots with Enhanced Relaxivity for Tumor Imaging. Nano Lett. [Internet]. Jan 9;19(1):441–8. Available from: https://doi.org/10.1021/acs.nanolett.8b04252

Younis YS, Ali AH, Alhafidhb OKS, Yahia WB, Alazzam MB, Hamad AA et al Early Diagnosis of Breast Cancer Using Image Processing Techniques. Velmurugan P, editor. J. Nanomater. [Internet]. 2022 Mar 30;2022:1–6. Available from: https://www.hindawi.com/journals/jnm/2022/2641239/

Zhang RR, Schroeder AB, Grudzinski JJ, Rosenthal EL, Warram JM, Pinchuk AN et al (2017) Beyond the margins: real-time detection of cancer using targeted fluorophores. Nat. Rev. Clin. Oncol. [Internet]. Nature Publishing Group; Jun 17;14(6):347–64. Available from: https://doi.org/10.1038/nrclinonc.2016.212

Publisher's Note